

Study of galaxies in the Lynx-Cancer void

VI. H_I-observations with the Nançay Radio Telescope

S.A. Pustilnik^{1, 2} and J.-M. Martin^{3, 4}

¹ GEPI, Observatoire de Paris, Place Jules Janssen, 92195 Meudon, France
e-mail: sap@sao.ru

² Special Astrophysical Observatory of RAS, Nizhnij Arkhyz, Karachai-Circassia 369167, Russia

³ GEPI, Observatoire de Paris, PSL Research University, CNRS, Univ Paris Diderot, Sorbonne Paris Cité, Place Jules Janssen, 92195 Meudon, France

⁴ Station de Radioastronomie de Nançay, Observatoire de Paris, CNRS, F-18330 Nançay, France
e-mail: jean-michel.martin@obspm.fr

Received January 19, 2016; accepted July 26, 2016

ABSTRACT

Context. Void population consists mainly of late-type and low surface brightness (LSB) dwarf galaxies whose atomic hydrogen is the main component of their baryonic matter. Therefore, observations of void galaxy H_I are mandatory in order to understand their evolution and dynamics.

Aims. Our aim was to obtain integrated H_I parameters for a fainter part of the nearby Lynx-Cancer void galaxy sample (total of 45 objects) with the Nançay Radio Telescope (NRT) and to conduct the comparative analysis of all the 103 void galaxies with known H_I data with a sample of similar galaxies residing in denser environments of the Local Volume.

Methods. For H_I observations we used the NRT with its sensitive antenna/receiver system FORT and standard processing. The comparison of the void and control samples on the parameter $M(\text{H I})/L_B$ is conducted with the non-parametric method, “The 2×2 Contingency Table test”.

Results. We obtained new H_I data for about 40 % of the Lynx-Cancer galaxy sample. Along with data from the literature, we use these new data for further analysis of 103 void objects. The proxy of the evolutionary parameter $M(\text{H I})/L_B$ of the void sample is compared with that of 82 galaxies of morphological types 8–10 residing in the Local Volume (LV) groups and aggregates.

Conclusions. At the confidence level of $P = 0.988$, we conclude that for the same luminosity, these void galaxies are systematically gas-richer, on average by ~39%. This result is consistent with the authors’ earlier conclusion on the smaller gas metallicities and evidence for the slower low-mass galaxy evolution in voids.

Key words. galaxies: dwarf – galaxies: evolution – galaxies: distances and redshifts – radio lines: galaxies – cosmology: large-scale structure of Universe

1. Introduction

Low-mass galaxies are thought to be the most fragile with respect to both internal and external perturbations of various origin (interactions, inflows, mergers) (e.g. Dekel & Silk 1986, Babul & Rees 1992). Therefore it is expected that their evolution is most sensitive to various kinds of galaxy collisions (e.g. distant tids, close pass-bys, major and minor mergers). Thus, it may significantly depend on the mean galaxy number density of various classes of the large-scale structure. Indeed, the strongest effects of dense environment on low-mass galaxy properties are found in galaxy clusters (e.g. Boselli et al. 2014 and references therein). In this scheme, if external perturbations play a substantial role in the secular evolution of typical dwarf galaxies, it is expected that at least the part of the dwarf galaxies located in voids could be less evolved objects.

In addition, studies of gravitational instabilities in the CDM cosmology indicate that low-mass haloes become bound later in the underdensity regions (low gravitational potential; e.g. Einasto et al. 2011). This is connected with the appearance of a bias in the Gaussian peaks formalism for the structure formation (Bardeen et al. 1986, Dekel & Silk 1986). This, in turn, could

also favour the appearance of less evolved low-mass galaxies in voids.

The study of galaxies in voids was quite popular during the last decade (Rojas et al. 2005, Patiri et al. 2006, Sorrentino et al. 2006, Kreckel et al. 2012, Beygu et al. 2012, among others), thanks to the emerging large sky surveys like the Sloan Digital Sky Survey (SDSS) and the Two-degree Field Galaxy Redshift Survey (2dFGRS). However, most of the studies of void galaxies mentioned above are mainly devoted to large and rather distant ($D \gtrsim 80\text{--}100$ Mpc) voids. This last choice, coupled with the demand of statistically complete galaxy samples (based on the apparent magnitude limit), limits the deepness of their void galaxy samples at the level of $M_B(M_r) \lesssim -17$.

Some differences between void and wall galaxies in this luminosity range have been found. In particular, void objects show a higher proportion of blue galaxies and higher star formation rates (SFR) (e.g. Rojas et al. 2004, 2005, and Hoyle et al. 2005, 2012). Similar results were obtained in the recent cosmological simulations by Kreckel, Joungh and Cen (2011), which indicate that the effect of the global environment of voids and walls is rather subtle for more massive galaxies. They found evi-

dence, however, that less massive objects in voids can show signs of evolutionary youth.

In order to address the issue of void environment effect on low-mass galaxy evolution (for galaxies below the adequate mass/luminosity limit, e.g. at $M_B \sim -12$ or fainter), it is necessary to study samples of intrinsically faint objects. Having in mind the common apparent magnitude limits of the main wide-angle redshift surveys (equivalent to $B_{\text{tot}} \sim 18.0\text{--}18.5$), this implies the necessity to study objects closer than ~ 20 Mpc and located in the nearby voids which are adjacent to the Local Volume.

In Pustilnik & Tepliakova (2011, Paper I) we described the large galaxy sample in the nearby Lynx-Cancer void ($D_{\text{centre}} \sim 18$ Mpc) and presented their main known parameters. One of the tasks was to measure and analyse the evolutionary parameters of void galaxies: metallicity (or gas-phase O/H) and gas mass-fraction. In the published version, there are 79 galaxies with the absolute magnitudes M_B in the range $[-12, -18.4]$, with a median of -14.0 , and with the substantial incompleteness at the fainter luminosities. Roughly half of the void sample galaxies are low surface brightness (LSB) galaxies, with extinction and inclination corrected central SB values of $\mu_{0,B,i} \geq 23.0^m/\square''$.

In Papers II and VII (Pustilnik et al. 2011a, 2016), we present a study of O/H in 81 members of the Lynx-Cancer void sample. We compared the data with the parameter O/H of similar galaxies in denser environments. Void galaxies appear to have systematically lower O/H (by about $\sim 37\%$ in average) for the same luminosities. Other studies show that $\sim 20\%$ of void LSB Dwarf galaxies (Pustilnik et al. 2011b; Chengalur, Pustilnik 2013, Perepelitsyna et al. 2014) are very metal-deficient and/or extremely gas-rich, indicating that void environment is conducive to unevolved objects.

Most of the late-type dwarf galaxies located in the Lynx-Cancer and presumably in other nearby voids are LSB objects (e.g. Perepelitsyna et al. 2014, hereafter Paper IV). They are known to have a significant or dominant part of baryon mass in the form of cold neutral gas. To study the properties of this very important component of void galaxies, it is necessary to know their global H I parameters and, first of all, their H I mass in order to derive their second evolutionary parameter, the gas mass-fraction f_{gas} . Moreover, since in many void galaxies the neutral gas appears to be the main baryonic component, it is crucial to know its physical properties in order to understand galaxy dynamics and star formation. Unusual, very gas-rich, and metal-poor galaxies found in course of H I surveys, are good candidates for detailed H I mapping. Some of studies of very metal-poor dwarfs are presented in the papers of Chengalur et al. (2006) and Ekta et al. (2006, 2008, 2009).

For half of the void galaxy sample (mainly for the brighter, more massive ones), the global H I parameters were known from various published sources (mainly from Haynes et al. 2011, Springob et al. 2005, Huchtmeier & Richter 1989, Swaters et al. 2002, and Begum et al. 2008). For the remaining void galaxies, we needed to conduct our own H I observations. Thus, the general goal of this work was to perform the most complete study of the void galaxy H I-properties. In addition, having the first results of such a study, there was a hope to find new unusual very gas-rich dwarfs among the fainter part of the void objects.

Some very interesting void low surface brightness dwarfs (LSBDs), namely very low metallicity and/or very gas-rich ones, were presented in Pustilnik et al. (2010, 2011b), Chengalur & Pustilnik (2013), and Chengalur et al. (2015). As the data in Paper I show, the Lynx-Cancer void galaxies have a rather small radial velocity dispersion. This is interesting by itself in order

to make a comparison with cosmological simulations. This also relates directly to the identification of void filaments. Since H I velocities are in general substantially more accurate than optical ones, they provide an additional opportunity to address the issues mentioned above.

Here we present all the NRT observed galaxies with known radial velocities from the updated (relative to Paper I) void sample (Pustilnik et al. 2016, in preparation), which currently includes 108 objects satisfying the primary selection criteria of this sample.

2. Sample

In Table 1 we present the main parameters taken from NED¹, SDSS², or from the literature for all observed 45 void galaxies. New objects taken from the updated Lynx-Cancer void sample (Pustilnik et al. 2016, in preparation) are marked by an asterisk (also in Table 3). Table 1 is organized as follows: Col. 1 – short IAU-style name; Col. 2 – other name or prefix (SDSS, HIPASS, etc.); Col. 3 – galaxy type; Cols. 4 and 5 – Epoch J2000 R.A. and Dec; Col. 6 – heliocentric velocity from optical data (when available); Col. 7 – heliocentric velocity from H I data; Col. 8 – total B -band magnitude. In most cases, this value is calculated from the total g and r magnitudes following Lupton et al. (2005). These latter values are obtained in Paper IV on the photometry of the SDSS DR7 (Abazajian et al. 2009) images. For galaxies located outside of the SDSS footprint, the B -band magnitudes are adopted from Pustilnik & Tepliakova (2011) where respective references are given. The only exception is J0802+0525 for which its B -magnitude is estimated directly from its SDSS model g and r values since we were unable to perform own photometry owing to a nearby bright star; Col. 9 – respective absolute magnitude, corrected for the Galaxy extinction A_B according to Schlafly & Finkbeiner (2011). The adopted distances are based on heliocentric velocities $V(\text{H I})$ from Table 2. They are calculated according to the prescriptions given in Paper I, accounting for the large peculiar velocity in this region $\Delta V \sim -300 \text{ km s}^{-1}$ (Tully et al. 2008). For a few objects, distances were determined using the velocity-independent methods (mainly Tip of RGB); Col. 10 – alternative name for the galaxy.

3. Observations and reduction

The H I observations were made during the period 2007–2013 with the Nançay radio telescope (NRT). The NRT has a collecting area of 200×34.5 m and a half-power beam width (HPBW) of $3.7'$ (east-west) \times $22'$ (north-south) at 21-cm and for a declination of $\delta=0^\circ$ (see <http://nrt.obspm.fr>). A cooled 1.1–1.8 GHz dual-polarization receiver and a 8192-channel autocorrelation spectrometer were used for the observation of the H I line. The system temperature was about 35 K and the conversion factor of the antenna temperature to the flux density for a point source was 1.5 K Jy^{-1} near the equator. The spectrometer covered a velocity range of about 2700 km s^{-1} , providing a channel spacing of 1.3 km s^{-1} before smoothing. The effective resolution after averaging four adjacent channels and Hanning smoothing was $\approx 10.4 \text{ km s}^{-1}$. Observations were obtained in separate cycles of ‘ON-source’ and ‘OFF-source’ integrations, each of 40 or 60 seconds in duration. OFF integrations were acquired at the target declination, with R.A. offset by $\sim 15' \times \cos(\delta)$ to the east.

¹ NASA/IPAC Extragalactic Database (NED)

² Sloan Digital Sky Survey (Abazajian et al. 2009 and references therein).

A noise diode was used to perform flux density calibration. Its power was regularly monitored through the observations of known continuum and line sources. The comparisons of our measured fluxes with independent measurements of the same objects with other telescopes indicates that flux density scales are consistent within 10%.

With the rms noise of ~ 1.5 to 5 mJy per resolution element after smoothing (10.4 km s^{-1}), we achieved a S/N ratio for the peak flux densities F_{peak} of the detected galaxies of 20–30 for the brightest objects, while for the faintest sources we had detections with a S/N ratio of only ~ 2.5 –4. Total integration times per galaxy (ON+OFF+pointing time) varied between 0.6 and 6 hours. For 3 of the 45 observed Lynx-Cancer void galaxies we only obtained upper limits of their F_{peak} and of their H I flux.

Primary data reduction was made with the standard NRT program *NAPS* written by the telescope staff. The follow-up data processing was done with the IRAM package *CLASS*. Both horizontal and vertical polarization spectra were calibrated and processed independently. They were finally averaged together. The baselines were generally well fitted by a third-order or lower polynomial and were subtracted out. Comments on the noise estimates and on several marginally detected or undetected void galaxies of the 45 observed are given in the next section.

4. Results

Table 2 presents the H I parameters derived from the observations. This is organized as follows: Col. 1 – short IAU-style name; Col. 2 – heliocentric velocity of the detected H I line with its 1σ error, in km s^{-1} . This is determined as the midpoint between the half-peak points on both sides of the H I profile; Col. 3 – the adopted distance as in Paper I (see comment for Col. 9 in Table 1); Cols. 4 and 5 – velocity widths in km s^{-1} of the H I profile at 50% and 20% of peak, W_{50} , W_{20} with their 1σ errors. They are determined as the velocity range between the respective points on both sides of the H I profile; Col. 6 – $F(\text{H I})$ – integrated flux of detected H I signal with its 1σ error in Jy km s^{-1} . Formulae for error estimates of parameters in Cols. 2, 4–6 were adopted from our earlier NRT H I survey (Thuan et al. 1999), which in turn uses the prescriptions from Schneider et al. (1990); Col. 7 – logarithm of total mass $M(\text{H I})$ in units of solar mass with its 1σ error; Col. 8 – ratio of $M(\text{H I})/L_B$ with related 1σ error, in solar units; Col. 9 – total time ON-source in minutes; Col. 10 – rms of noise near the H I peak in mJy at the velocity resolution of 10.4 km s^{-1} ; Col. 11 – signal-to-noise ratio for peak value of the respective H I profile.

Figures 1 and 2 show in order of increasing R.A. the H I profiles of the void galaxies listed respectively in Table 1 and Table 2. For the triplet of MRK 407 (J094747.60+390503.0) only two H I profiles are presented; they are rather complex and were obtained with the NRT beam pointing in the direction of the largest members of the triplet. In addition, H I profile of the galaxy J090018.30+322226.2 is not shown since no signal was detected. Therefore, the total number of profiles displayed is 43. We present below our comments about some peculiar objects.

SDSS J072301.42+362117.1 and *J072313.46+362213.0*. The first galaxy, a LSB dwarf, has been identified as a new Lynx-Cancer void galaxy after its redshift was obtained at the SAO 6m telescope (BTA). Its NRT H I profile suggested a possible contribution from a nearby galaxy which has been found as a very low surface brightness dwarf, $\sim 2^m$ fainter than the main component, at $\sim 3'$ to E (J072313.46+362213.0). An additional NRT observation in the direction partly disentangled the confusion between

the H I contributions. The final H I parameters for these two galaxies and a third even fainter one (J072320.57+362440.8, see Table 3) have been adopted after the subsequent GMRT H I mapping of this triplet (Chengalur, Pustilnik 2013).

SDSS J080238.15+052551.2. This very faint and compact optical object close to a bright star was included in the void sample after its assumed identification with a faint ALFALFA source (Haynes et al. 2011) with $V(\text{H I})=830 \text{ km s}^{-1}$, $F(\text{H I})=0.43 \pm 0.04 \text{ Jy km s}^{-1}$ with S/N ratio of 6.2 (AGC 188988). With such parameters, this galaxy has a very high ratio $M(\text{H I})/L_B \sim 4.8$ (using the total SDSS g and r magnitudes, transformed to $B_{\text{tot}}=19.8$). Since very gas-rich galaxies are rare objects, we conducted H I observations of AGC 188988 with the NRT. Our NRT data indicate no signal at the respective velocity with an upper limit of $F(\text{H I}) < 0.16 \text{ Jy km s}^{-1}$ (2σ).

The probable interpretation of this case is a false ALFALFA detection. If, however, there is H I associated with the suggested faint optical object, its ratio $M(\text{H I})/L_B < 1.8$ is not so large. We consider this object's data to be unreliable and excluded it from the following statistical analysis.

SDSS J090018.30+322226.2. This galaxy is a new void object with $V_{\text{hel}} = 740 \pm 30 \text{ km s}^{-1}$, as measured on the faint H α emission in the spectrum obtained at the BTA. At NRT the signal at this radial velocity is within 1.4σ , so the numbers below should be treated as upper limits. With $W_{50} = 30 \text{ km s}^{-1}$, typical of galaxies with $M_B \sim -12$, which results in the total flux of $0.14 \pm 0.10 \text{ Jy km s}^{-1}$. For parameter $M(\text{H I})/L_B$ the respective value is 0.72 ± 0.52 .

SDSS J094003.27+445931.7. This galaxy has marginally detected H I with the radial velocity close to that derived from the SDSS emission-line spectrum ($1358 \pm 4 \text{ km s}^{-1}$). However, there is also a similar flux detection (at the level of $\sim (2-3)\sigma$) at $V_{\text{hel}} = 1202 \pm 8 \text{ km s}^{-1}$. The search for a possible optical counterpart on the SDSS image to this H I component produced two candidates within the NRT beam.

The nearest one is a small and almost edge-on blue disc SDSS J093951.28+445921.9 with $g=19.34$, $r=19.15$. Its BTA spectrum has revealed the velocity of the H α line of $\sim 14000 \text{ km s}^{-1}$. The second candidate is the almost face-on LSB disc SDSS J093950.11+444800.1 with $g=17.55$, $r=17.18$ ($B \sim 17.90$), $\sim 11.5'$ to the south and 13.16 s ($\sim 140''$) to the west. Owing to the NRT beam offset, its nominal H I-flux should drop by a factor of 6.5. In this case, its ratio $M(\text{H I})/L_B$ is ~ 1.4 , rather typical of void LSBs. The optical redshift of this galaxy is needed in order to fix the origin of the second H I source.

MRK 407=J094747.60+390503.0. This blue compact galaxy (BCG) is the brightest member of a triplet, which also includes ~ 1.7 mag fainter LSB UZC J09475+3908 at $3'$ to the north and ~ 3 mag fainter LSB SDSS J094758.45+390510.1 at $\sim 2'$ to the east. Each galaxy contributes to the $F(\text{H I})$ for any NRT pointing in the direction of the triplet. We used our NRT results, accounting for the a priori known decrease of H I flux for the sources NRT beam offset, as well as the earlier observations of MRK 407 by Thuan & Martin (1981) to disentangle the contribution of each component of the triplet. The typical estimated accuracy of the resulted $F(\text{H I})$ is $\sim 20\%$. Follow-up GMRT mapping of this triplet (Chengalur et al., in preparation) will give a better understanding of its properties.

SDSS J095633.65+271659.3 with $V_{\text{hel}} = 1059 \text{ km s}^{-1}$ is a faint companion of a $\sim 4^m$ brighter spiral IC 2520 (at 13.2° to the west and $3.3'$ to the south, see Table 3), which is also in the NRT beam and is seen in the plot of the H I profile as an additional peak at $V_{\text{hel}} = 1243 \text{ km s}^{-1}$.

SDSS J101014.96+461744.1. This is a faint galaxy with a good S/N SDSS emission-line spectrum. Its optical redshift corresponds to $V_{\text{hel}} = 1092 \pm 3 \text{ km s}^{-1}$. On our data, there is no detectable H α flux, for $\sigma_{\text{noise}} \sim 2.4 \text{ mJy}$. For statistical analysis, we adopt for its F the upper limit $F(\text{H}\alpha) < 0.12 \text{ Jy km s}^{-1}$ and the value of $M(\text{H}\alpha)/L_B < 0.34$.

5. Analysis

In our analysis of the properties of the Lynx-Cancer void galaxy sample, we use the optical parameters gathered from the literature, as mentioned in section 2, and the H α parameters obtained from our observations or taken from the literature. Table 3 lists galaxies with H α data taken from the literature, with their H α and optical parameters. Table 3 is organized as follows: Cols. 1 to 5 – same as Table 1; Col. 6 – adopted heliocentric velocity V_{hel} ; Cols. 7 and 8 – the total apparent and absolute B magnitudes: for the published sample outside the SDSS zone, from Paper I; for galaxies with new photometry, from the papers by Perepelitsyna et al. (2014); and for the rest of the updated version of the void sample, from Pustilnik et al. (2016, in preparation). The few exceptions are the following. For J0706+3620 and UGC 3672, their B magnitudes are adopted from Chengalur et al. (2016). For J0736+0959, its B magnitude is adopted from the recent photometry in Haurberg et al. (2015). For J0956+2900 (DDO68C), there is no possibility of estimating its optical flux because of a nearby bright star. We adopt its B magnitude based on $M(\text{H}\alpha)$ in Cannon et al. (2014) and a typical of this sample value of $M(\text{H}\alpha)/L_B = 1$; Cols. 9 and 10 – total H α flux $F(\text{H}\alpha)$ and derived $M(\text{H}\alpha)$; Col. 11 – reference to the H α data. In total, we use the data of 103 void galaxies in this analysis.

In order to compare the gas-content parameter $M(\text{H}\alpha)/L_B$ of the void sample with that of a sample of galaxies in denser environments, we created a sample of 82 late-type dwarf and subluminal galaxies in the LV residing in groups and the Canes Venatici I (CVnI) cloud. The latter were described by Karachentsev (2005). We used those members of these groups for which we found H α data in the literature, mainly in the Catalog of Nearby Galaxies (CNG) by Karachentsev et al. (2004).

We show the distributions of parameter $M(\text{H}\alpha)/L_B$ for the void and the LV-groups samples in Figure 3 (top and bottom left panels, respectively). The median value of $M(\text{H}\alpha)/L_B$ for the combined void and LV-group sample of 185 galaxies is equal to 1.01. Therefore, galaxies with $M(\text{H}\alpha)/L_B \geq 1.0$ are denoted ‘gas-rich’. Although each sample shows rather large scatter (indicating that there are several affecting factors), the distribution of the void galaxies is confidently shifted to the higher values of $M(\text{H}\alpha)/L_B$. This effect is apparent in a factor of ~ 1.39 difference between their medians (1.21 and 0.87, respectively) and the significant difference in fractions of gas-rich objects in the void and LV-groups samples (0.59 and 0.41). Since these differences might be due to the statistical scatter, more advanced statistical tests are needed.

The significance of the second difference can be tested via non-parametric statistical methods. In particular, we use a test well known in biology and quality control, called The 2 \times 2 Contingency Table test (e.g. Bol’shev and Smirnov 1983, and references therein). It appears to be more powerful than the Kolmogorov–Smirnov test in problems like this, as was tested for a similar astronomical problem in Pustilnik et al. (1995, see the detailed Appendix). Here we briefly summarize the process of grouping the galaxies in the respective cells of Table 2 \times 2. The zero hypothesis H_0 states that the property G being ‘gas-rich’ does not relate to the property V belonging to the void environ-

ment, or in other words, the fraction of gas-rich galaxies is the same for both compared samples of late-type galaxies. The respective Table 2 \times 2 reads as follows:

Property	G	non- G	Sum 1
V	$m=61$	$n-m=42$	$n=103$
non- V	$M-m=34$	$N-n-(M-m)=48$	$N-n=82$
Sum 2	$M=95$	$N-M=90$	$N=185$

Here $m=61$ is the number of void gas-rich galaxies and $n-m=42$ is the number of void non-gas-rich objects; $M-m=34$ is the number of non-void gas-rich galaxies, while $N-n-(M-m)=48$ is the number of non-void non-gas-rich ones. If properties G and V were independent, that is, if there were no correlation between the property of belonging to void and the property of being gas-rich, the probability of accidentally getting a table with the same occupation numbers [61, 42, 34, 48], calculated according to the formulae in the above Appendix (and Bol’shev and Smirnov 1983) is less than $p = 0.012$. The respective probability of rejecting H_0 with the given occupation numbers is $P = 1 - p = 0.9882$. Hence, the visual impression on the significantly higher fraction of void gas-rich objects is supported by the statistical criterion at the confidence level P of 0.9882.

In addition to the distributions on parameter $M(\text{H}\alpha)/L_B$, in the right-hand panels of Fig. 3 we also compare its relation to galaxy luminosity (via parameter M_B). To aid the eye, we draw upper boundary straight lines for both samples. The visual inspection shows that for the Lynx-Cancer void galaxies this upper line goes slightly higher (by a factor of 1.6–2.0) than for ‘group’ galaxies in the whole range of galaxy luminosities. The same is valid for the bottom boundary. With only one exception, the most gas-poor void galaxies have substantially higher values of $M(\text{H}\alpha)/L_B$ than the similar galaxies in groups.

6. Discussion

In discussing noticeable differences in the gas content between void and group late-type galaxies, it is important to pay attention that the group sample is itself quite inhomogeneous, including the classical Local Volume groups similar to our own Local Group (M81, CenA, M83, IC 342, Maffei, Scu) one rather rarefied and unrelaxed aggregate known as the CVnI cloud. It is curious and instructive that three of the six most gas-rich galaxies in the group sample ($M(\text{H}\alpha)/L_B = 4.3 - 6.9$) belong to the outer parts of this aggregate, and hence can be treated as falling to this from the lower-density environment. These most gas-rich galaxies include DDO 154, UGCA 292, and UGC 3741 with respective values of parameter $M(\text{H}\alpha)/L_B$ of 4.5, 6.9, and 4.3 (see the recent summary in Chengalur, Pustilnik 2013). The structure of the CVnI cloud was revisited by Makarov, Makarova and Uklein (2013), based on the improved TRGB distance determinations.

The above-mentioned extreme members of the CVnI cloud reside far from the centre of the cloud, closer to the zero-velocity radius ($R=1.06 \text{ Mpc}$) or substantially further (at $\sim 1.1, 0.9$, and 1.6 Mpc , respectively), and thus can probably be treated as being in the process of fall-off onto CVnI cloud. Coming from the significantly lower density environment, they can possess properties of some of the most unevolved representatives of underdense regions.

To check the effect of the CVnI cloud galaxies on the comparison of the LV vs Lynx-Cancer void galaxy samples, we have removed the 11 CVnI cloud galaxies from the whole Local Volume sample and are left with 71 LV galaxies. We apply the same

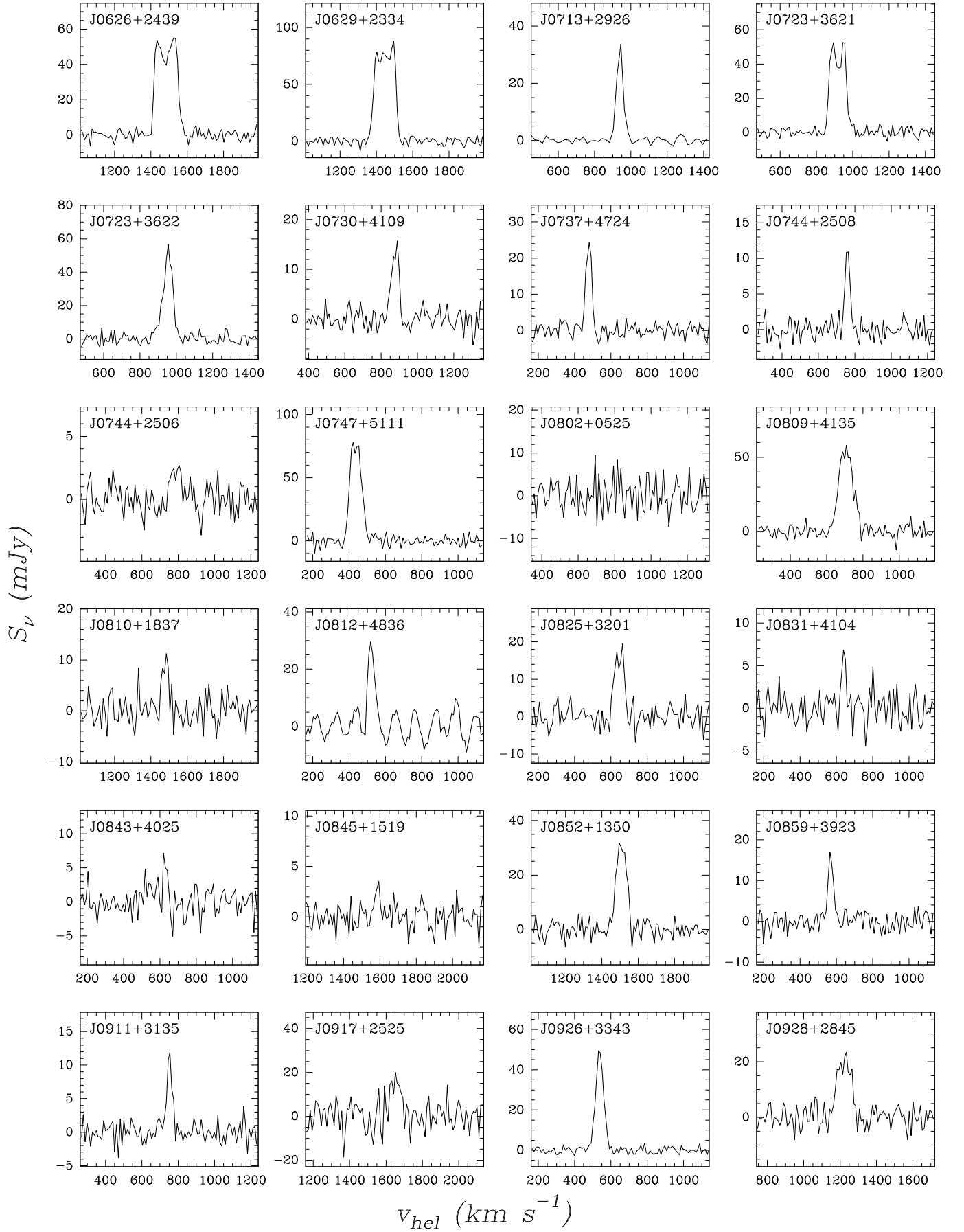


Fig. 1. NRT H I profiles S_ν (in mJy) vs V_{hel} (km s^{-1}) of all studied galaxies.

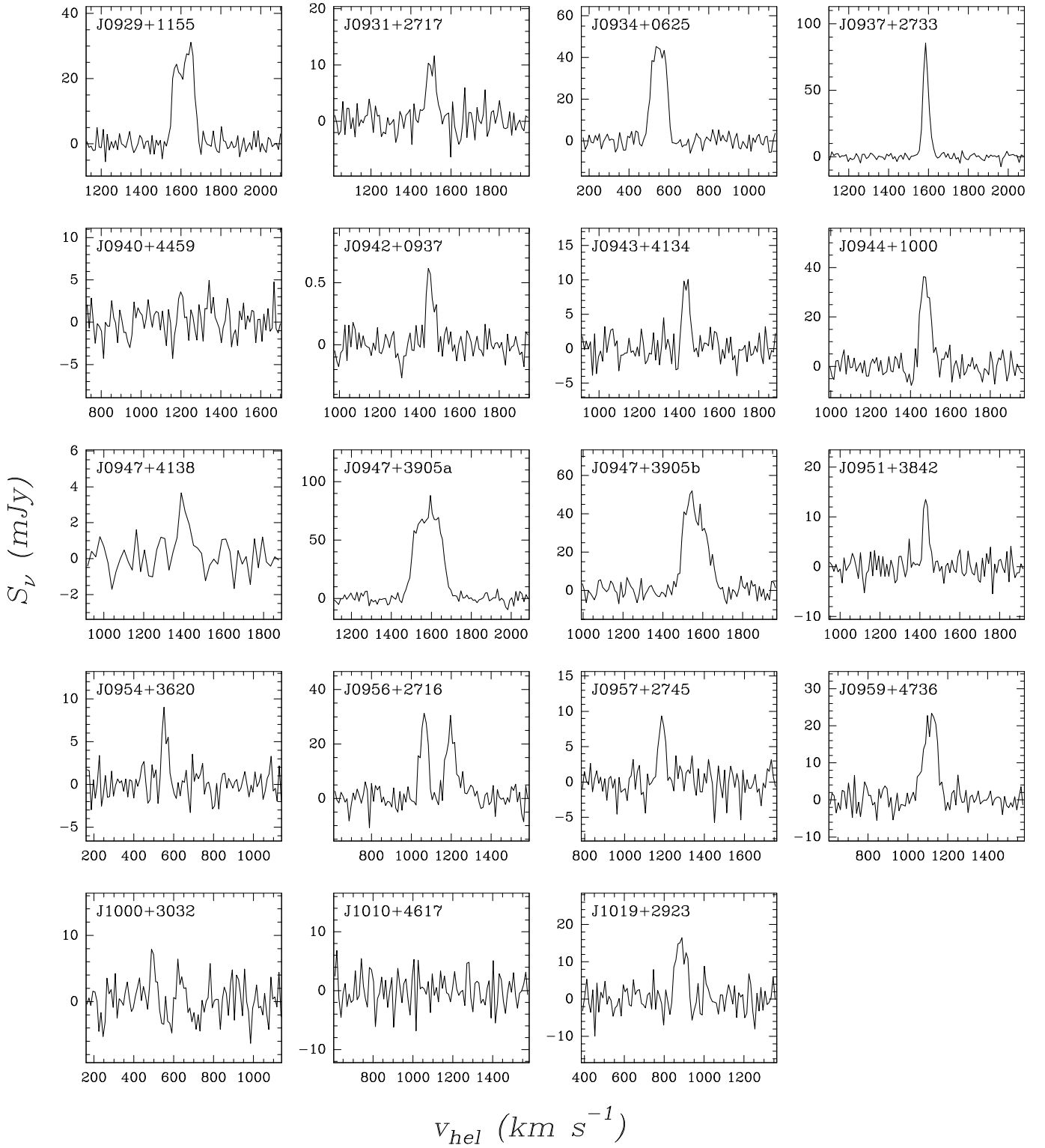


Fig. 2. NRT HI profiles S_ν (in mJy) vs V_{hel} (km s^{-1}) of all studied galaxies.

Table 2x2 method used above to check the null hypothesis H_0 on the independence of a gas-rich galaxy fraction on the type of environment. For the new table, the probability of accidentally getting the variant with occupation numbers [61, 42, 27, 44] is $p = 0.00444$, ~ 2.7 times smaller than for the whole Local Volume subsample. The respective confidence level to reject H_0 is $P = 1 - p = 0.99556$. This probably indicates that at least a part of the CVnI cloud galaxies are in a special evolutionary status.

One important note relates to the conclusion on the difference in distributions of parameter $M(\text{HI})/L_B$ for the void and group (Local Volume groups) samples. As can be seen in the right panels of Fig. 3, there is a trend (also known from several earlier works, see e.g. Huchtmeier et al. 1997; Pustilnik et al. 2002): the ratio $M(\text{HI})/L_B$ increases with the decrease in galaxy luminosity (see also Fig. 5 for the rate of this increase). Therefore, if the two samples under comparison differ significantly in

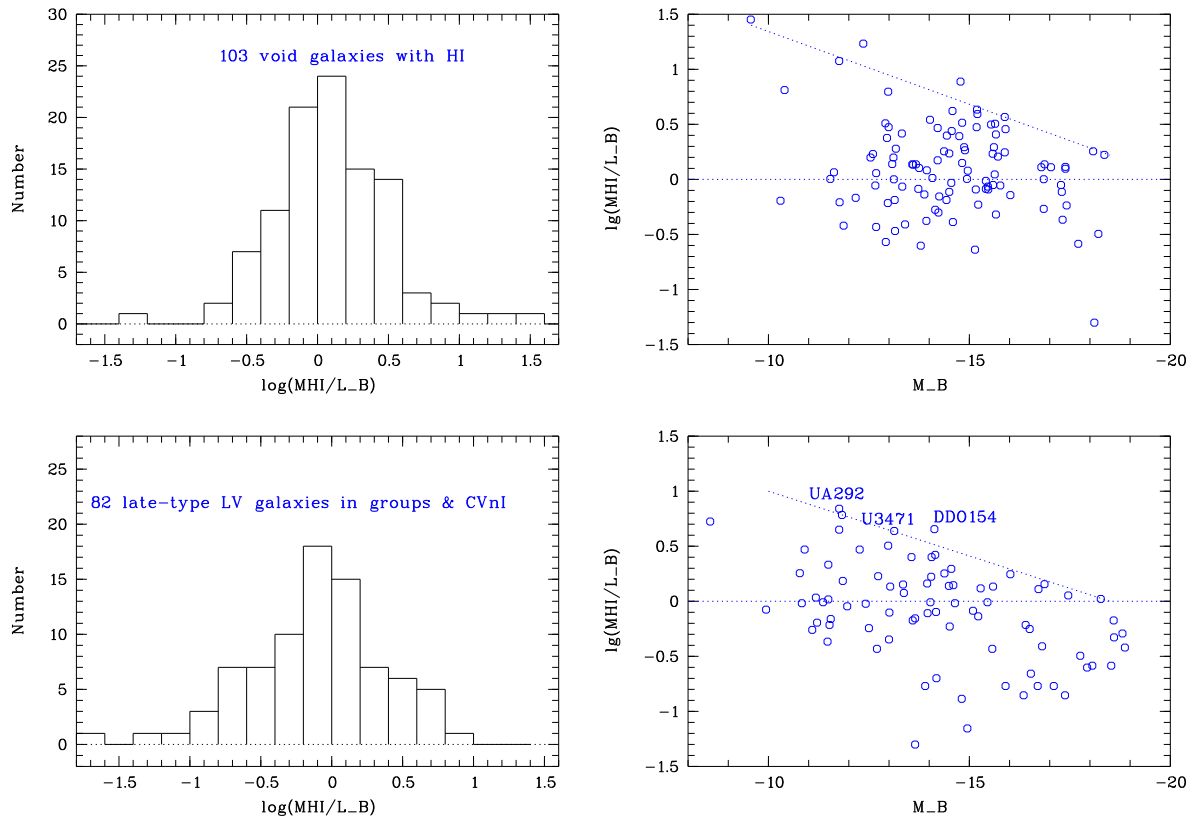


Fig. 3. **Top left:** Distribution of mass-to-light ratio $M(\text{HI})/L_B$ for all Lynx-Cancer void galaxies with HI data and **Top right:** Relationship between $M(\text{HI})/L_B$ and the absolute magnitude M_B . **Bottom left:** Distribution of $M(\text{HI})/L_B$ for late-type dwarf and subluminal galaxies in the Local Volume (LV) groups and the CVnI cloud from Karachentsev (2005). **Bottom right:** Relationship between $M(\text{HI})/L_B$ and the absolute magnitude M_B for the same late-type galaxy sample. The scatter of parameter $M(\text{HI})/L_B$ is large for all values of M_B , indicating the interplay of several significant factors. Nevertheless, the fraction of higher $M(\text{HI})/L_B$ ratio objects is clearly larger for void galaxies. Also, the three highest ratio galaxies from the LV sample are situated in the outer parts of groups and CVnI cloud (marked by their names). Median values of $M(\text{HI})/L_B$ are respectively, 1.21 and 0.87 for void and the LV ‘late-type in groups’ samples, which differ by a factor of ~ 1.39 . The upper boundary line for the void sample is also a factor of 1.6–2 higher than that for the ‘group’ sample.

M_B distribution, it is possible to obtain a noticeable difference in distribution $M(\text{HI})/L_B$, even though in reality these samples have the same distribution. In Figure 4 and with related numbers we show that this is not the case. Indeed, both distributions on M_B are similar, have close mean and median values of M_B (see numbers in the Figure legend), and are somewhat lower for the group sample. The latter should lead in general to the opposite effect, that is the group sample should have more numerous gas-rich galaxies.

In Fig. 5 we show how the galaxy hydrogen mass $M(\text{HI})$ is related to the blue luminosity L_B . The left panel is for the sample of 103 Lynx-Cancer void galaxies, while the right panel is for 82 galaxies of the Local Volume group sample. Dotted lines show the positions of galaxies with $M(\text{HI})/L_B=1$ (in solar units, with a slope of 1.0). The red dashed lines (see figure legend) show the real linear regression for considered samples. They indicate that for both samples, galaxies become on average gas-richer with decreasing luminosity. The respective coefficients in the relation $\log(M(\text{HI})/L_B)/\log(L_B)=-0.129\pm0.054$ (void sample) and -0.208 ± 0.051 (Local Volume sample) do not differ significantly. Thus, their average $\langle k \rangle = -0.163\pm0.040$ can be considered representative of such a relationship for both samples.

It is interesting to compare this result with estimates published for other samples. In particular, Staveley-Smith et al. (1992) found $k = -0.3\pm0.1$ for a sample of LSB dIs and BCGs, while Smoker et al. (2000) found $k = -0.2\pm0.1$ for emission-line

galaxies of the University of Michigan survey. In the Pustilnik et al. (2002) study of BCGs in various environments, this slope for non-cluster BCGs is consistent with average of $\langle k \rangle = -0.25\pm0.1$. Thus, within rather large scatter, all available data for late-type and BCG galaxies on the relation $M(\text{HI})/L_B \propto L_B^k$ are consistent with the common index $k \sim -0.2$. This corresponds to a factor of ~ 4 increase in $M(\text{HI})/L_B$ for a factor of 1000 decrease in luminosity.

This relation is a specific illustration of the well-known down-sizing phenomenon which is connected to the slower evolution of smaller mass galaxies. The general trend towards lower gas metallicity for smaller galaxies is a better-known manifestation of the same phenomenon.

6.1. Summary

1. NRT HI data are presented for 45 galaxies of the Lynx-Cancer void. Along with HI data already published in the literature, we were able to build a large sample of 103 galaxies and study the properties of $\sim 95\%$ of the updated Lynx-Cancer void galaxy sample.
2. The analysis of parameter $M(\text{HI})/L_B$ – observational proxy of the relative gas content – for the void galaxy sample revealed a significant excess (at the confidence level $P=0.988$) of gas-rich objects in the void sample with respect to similar late-type galaxies residing in the Local Volume (LV) groups and

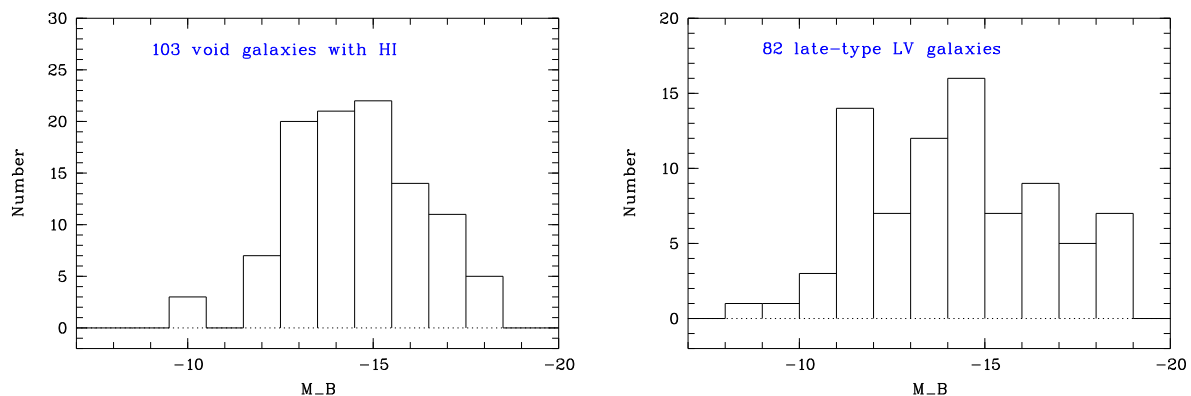


Fig. 4. Left: Distribution of M_B for 103 Lynx-Cancer void galaxies with HI data. **Right:** Same distribution of M_B for the comparison sample 82 galaxies in groups inside the Local Volume. Median and mean values of M_B of the groups sample (-14.10 and -14.24) are somewhat fainter than for the void sample (-14.45 and -14.61 , respectively). The standard deviation for the former, in contrast is somewhat higher (2.38 mag vs 1.83 mag). See the Discussion for further implications.

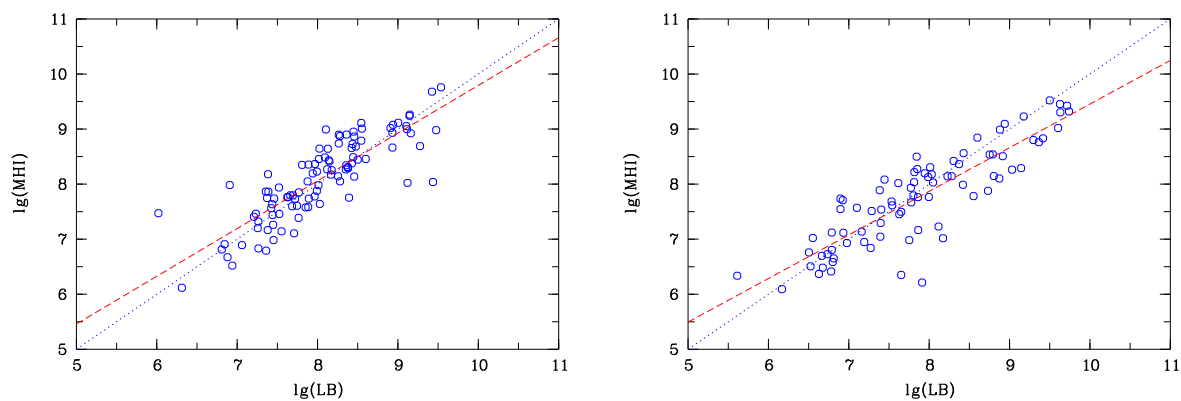


Fig. 5. Left: Relation between $M(\text{HI})$ and L_B (in solar units) for 103 Lynx-Cancer void galaxies with HI data. The dotted line shows positions for objects with $M(\text{HI})/L_B=1$. The dashed line shows the linear regression on all galaxies, with the slope of $k1=0.875\pm0.055$ and $\text{rms}=0.45$ (in $\log M(\text{HI})$). **Right:** Same relation for all 82 galaxies from the comparison sample in the Local Volume groups. The slope of the linear regression is $k2=0.792\pm0.051$ and $\text{rms}=0.44$ (in $\log M(\text{HI})$). See the Discussion for further implications.

in the CVnI cloud. For the LV group objects which do not belong to the CnVI cloud, the difference is significant at the confidence level of 0.9956.

3. This result can be treated as independent evidence for the slower evolution of typical void galaxies. This is consistent with similar conclusions previously published by the authors, based on the analysis of gas-phase metallicity in void galaxies and similar galaxies in denser environments.
4. The ratio $M(\text{HI})/L_B$ for the void galaxies has a broad distribution with extreme values of ~ 0.05 and ~ 28 , indicating that various competing factors can define the galaxy evolution in voids. The median value of $M(\text{HI})/L_B$ varies with M_B within a factor of ~ 4 (from ~ 0.5 to ~ 2) for a luminosity range of ~ 3 orders of magnitude.

Acknowledgements. We thank the NRT Program Committee for allocating time for this project during the years 2007 – 2012. The authors appreciate the anonymous referee’s report, which allowed us to improve the quality of the paper. The work of SAP was partly supported by RFBR grants No. 11-02-00261 and 14-02-00520. SAP appreciates the hospitality and support from the Paris Observatory and its laboratory GEPI during his visits for this project. We thank J. Chengalur for permission to use the HI-fluxes for UGC 3672 system components prior to publication. The Nançay Radio Observatory is the Unité scientifique de Nançay of the Observatoire de Paris, associated as Unité de Service et de Recherche (USR) No. B704 to the French Centre National de la Recherche (CNRS). The Nançay Observatory also gratefully acknowledges the financial support of the Conseil Régional de la Région Centre in France. This research has made use

of the NASA/IPAC Extragalactic Database (NED) which is operated by the Jet Propulsion Laboratory, California Institute of Technology, under contract with the National Aeronautics and Space Administration. We acknowledge the usage of the HyperLeda database (<http://leda.univ-lyon1.fr>, Paturel et al. 2003).

References

- Abazajian K.N., Adelman-McCarthy J.K., Agüeros M.A., et al., 2009, *ApJS*, 182, 543
- Babul A., Rees M.J. 1992, *MNRAS*, 255, 346
- Bardeen J.M., Bond J.M., Kaiser N., Szalay A.S., 1986, *ApJ*, 304, 15
- Begum A., Chengalur J.N., Karachentsev I.D., Sharina M.E., Kaisin S.S., 2008, *MNRAS*, 386, 1667
- Beygu B., Kreckel K., van de Weygaert R., van der Hulst J.M., van Gorkom J.H., 2012, *AJ*, 145, 120
- Bol’shev L.N. & Smirnov N.V., 1983, *Tables of Mathematical Statistics*, Moscow, Nauka Publishers.
- Boselli A., Voyer E., Boissier S., et al., 2014, *A&A*, 570, A69
- Cannon J.M., Johnson M., McQuinn K., et al., 2014, *ApJ*, 787, L1
- Chengalur J.N., Pustilnik S.A., 2013, *MNRAS*, 428, 1579
- Chengalur J.N., Pustilnik S.A., Martin J.-M., Kniazev A.Y., 2006, *MNRAS*, 371, 1849
- Chengalur J.N., Pustilnik S.A., Makarov D.I., Perepelitsyna Y.A., Safonova E.S., Karachentsev I.D., 2015, *MNRAS*, 448, 1643 (Paper V)
- Chengalur J.N., Pustilnik S.A., Egorova E.S., 2016, *MNRAS*(in press)
- Dekel A., Silk J., 1986, *ApJ*, 303, 39
- Einasto J., Suhhonenko I., Hutsi G., et al. 2011, *A&A*, 534, A128
- Ekta, Chengalur J.N., Pustilnik S.A., 2006, *MNRAS*, 372, 853

- Ekta, Chengalur J.N., Pustilnik S.A., 2008, MNRAS, 391, 881
- Ekta B., Pustilnik S.A., Chengalur J.N., 2009, MNRAS, 397, 963
- Haurberg N.C., Salzer J.J., Cannon J.M., Marshall M.V., 2015, ApJ, 800, article id. 121
- Haynes M., Giovanelli R., Martin A.M., et al. 2011, AJ, 142, 170
- Hirschauer A.S., Salzer J.J., Skillman E.D., et al., 2016, ApJ, 822, article id. 108
- Hoyle F., Rojas R.R., Vogeley M.S., Brinkmann J., 2005, ApJ, 620, 618
- Hoyle F., Vogeley M.S., Pan D., 2012, MNRAS, 426, 3041
- Huchtmeier W.K., and Richter O.-G., A General Catalog of HI Observations of Galaxies, 1989, New York: Springer-Verlag
- Huchtmeier W.K., Hopp U., Kuhn B., 1997, A&A, 319, 67
- Karachentsev I.D., 2005, AJ, 129, 178
- Karachentsev I.D., Karachentseva V.E., Huchtmeier W.K., 2001, A&A, 366, 428
- Karachentsev I.D., Karachentseva V.E., Huchtmeier W.K., Makarov D.I., 2004, AJ, 127, 2031
- Kreckel K., Jounge M.R., Cen R. 2011, ApJ, 735, 132
- Kreckel K., Platen E., Aragon-Calvo M.A., van Gorkom J.H., van de Weygaert R., van der Hulst J.M., Beygu B., 2012, AJ, 144, 16
- Lupton R., et al. 2005, <http://www.sdss.org/dr5/algorithms/sdssUBVRITransform.html#Lupton2005>
- Makarov D.I., Makarova L.N., Uklein R.I., 2013, Astrophys.Bulletin, 68, N.2, 125 (arXiv:1305.3701)
- Matthews L.D., van Driel W., 2000, A&AS, 143, 421
- Matthews L.D., Uson J.M., 2008, AJ, 135, 291
- O'Neil K., 2004, AJ, 128, 208
- Patiri S.G., Prada F., Holtzman J., Klypin A., Betancort-Rijo J., 2006, MNRAS, 372, 1710
- Patuarel G., Petit C., Prugniel P., Theureau G., Rousseau J., Brouty M., Dubois P., Cambr sy L., 2003, A&A, 412, 45
- Perepelitsyna Y.A., Pustilnik S.A., Kniazev A.Y., 2014, Astrophys.Bulletin, 69, 247 (Paper IV) (arXiv:1408.0613)
- Popping A., Braun R., 2011, A&A, 528A, 28
- Pustilnik S.A., Martin J.-M., 2007, A&A, 464, 859
- Pustilnik S.A., Tepliakova A.L., 2011, MNRAS, 414, 1188 (Paper I)
- Pustilnik S.A., Ugryumov A.V., Lipovetsky V.A., Thuan T.X., Guseva N.G., 1995, ApJ, 443, 499
- Pustilnik S.A., Martin J.-M., Huchtmeier W., Brosch N., Lipovetsky V.A., Richter G.M., 2002, A&A, 389, 405
- Pustilnik S.A., Tepliakova A.L., Kniazev A.Y., Burenkov A.N., 2010, MNRAS, 401, 333
- Pustilnik S.A., Tepliakova A.L., Kniazev A.Y., 2011, Astrophys.Bulletin, 66, 255 (Paper II, arXiv:1108.4850)
- Pustilnik S.A., Martin J.-M., Tepliakova A.L., Kniazev A.Y., 2011, MNRAS, 417, 1335 (Paper III)
- Pustilnik S.A., Perepelitsyna Y.A., Kniazev A.Y., 2016, MNRAS, DOI 10.1093/mnras/stw2039, in press (Paper VII)
- Rojas R.R., Vogeley M.S., Hoyle F., Brinkmann J., 2004, ApJ, 617, 50
- Rojas R.R., Vogeley M.S., Hoyle F., Brinkmann J., 2005, ApJ, 624, 571
- Schlafly E.F., Finkbeiner D.P., 2011, ApJ, 737, art. id. 103
- Schneider S.E., Thuan T.X., Magri C., Wadiak J.E., 1990, ApJS, 72, 245
- Schneider S.E., Thuan T.X., Mangum J.G., Miller J., 1992, ApJS, 81, 5
- Smoker J.V., Davies R.D., Axon D.J., Hummel E., 2000, A&A, 361, 19
- Sorrentino G., Antonuccio-Delogu V., Rifatto A., 2006, A&A, 460, 673
- Springob C.M., Haynes M.P., Giovanelli R., Kent B.R., 2005, ApJS, 160, 149
- Staveley-Smith L., Davies R.D., Kinman T.D., 1992, MNRAS, 258, 334
- Swaters R.A., van Albada T.S., van der Hulst J.M., Sancisi R., 2002, A&A, 390, 863
- Thuan T.X., Martin G.E., 1981, ApJ, 247, 823
- Thuan T.X., Lipovetsky V.A., Martin J.-M., Pustilnik S.A., 1999, A&A Suppl.Ser., 130, 100
- Tully R.B., Shaya E.J., Karachentsev I.D., Courtois H.M., Kocevski D.D., Rizzi L., Peel A., 2008, ApJ, 676, 184

Table 1. Parameters of the Lynx-Cancer void sample galaxies observed with NRT

Short IAU style name	Other name or prefix	Type	Coord. (2000.0)		V_{opt} km s ⁻¹	$V(\text{HI})$ km s ⁻¹	$B_{\text{tot}}^{\ddagger}$ mag	M_{B}^{0*} mag	Alternative name
			R.A. <i>h m s</i>	Dec. <i>° ' "</i>					
(1)	(2)	(3)	(4)	(5)	(6)	(7)	(8)	(9)	(10)
J0626+2439	HIPASS	Scd	06 26 20.97	+24 39 20.0	1473±7	1485±2	17.98	-15.64	PGC1689759
J0629+2334	HIPASS	Scd	06 29 58.23	+23 34 28.5	1452±6	1445±3	17.10	-15.88	
J0713+2926*	SDSS	dI?	07 13 05.15	+29 26 42.8	...	938±2	16.79	-14.55	
J0723+3621	SDSS	Sm?	07 23 01.42	+36 21 17.1	888±2	917±2	17.01	-14.21	
J0723+3622	SDSS	LSB	07 23 13.46	+36 22 13.0	954±3	970±5	19.46	-11.76	
J0730+4109	SDSS	dI?	07 30 58.90	+41 09 59.8	874±3	878±5	16.67	-14.59	MCG 9-13-56
J0737+4724	SDSS	LSB	07 37 28.47	+47 24 32.8	404±60	474±5	18.02	-12.54	
J0744+2508	SDSS	dI	07 44 43.72	+25 08 26.6	749±4	760±3	18.11	-12.66	
J0744+2506*	SDSS	dI	07 44 55.52	+25 06 01.8	778±99	752±6	20.47	-10.30	
J0747+5111	SDSS	Sm	07 47 32.10	+51 11 29.0	454±84	433±3	15.12	-15.16	
J0802+0525 ⁽¹⁾	SDSS	Comp	08 02 38.15	+05 25 51.2	830±23	824±6	19.80	-10.93	AGC 188988
J0809+4135	SDSS	Sd?	08 09 36.10	+41 35 40.0	704±50	712±5	15.46	-15.41	MCG 7-17-19
J0810+1837	SDSS	Sm:	08 10 30.65	+18 37 04.1	1495±37	1481±8	18.39	-13.58	KUG 0821+321
J0812+4836	SDSS	dI	08 12 39.53	+48 36 45.4	521±5	522±4	17.36	-13.08	
J0825+3201	SDSS	Ir	08 25 04.90	+32 01 05.1	648±16	647±6	16.91	-13.73	
J0831+4104	SDSS	LSB	08 31 41.21	+41 04 53.7	582±40	640±3	17.71	-12.92	
J0843+4025	SDSS	Im	08 43 37.98	+40 25 47.2	614±3	627±10	17.90	-12.68	
J0845+1519	SDSS	dI	08 45 25.40	+15 19 46.0	1642±50	1584±12	18.61	-13.40	HS 0944+4152
J0852+1350	SDSS	LSB	08 52 33.75	+13 50 28.3	1511±4	1502±8	17.40	-14.56	
J0859+3923	SDSS	dI	08 59 46.93	+39 23 05.6	588±34	568±3	17.25	-13.14	
J0900+3222*	SDSS	dI	09 00 18.30	+32 22 26.2	740±30	...	18.97	-11.77	
J0911+3135	SDSS	dI	09 11 59.43	+31 35 35.9	750±4	753±6	18.05	-12.68	
J0917+2525	IC2450	S0	09 17 05.27	+25 25 44.9	1644±2	1643±12	14.06	-18.11	PC 0956+4751
J0926+3343	SDSS	Sm:	09 26 09.45	+33 43 04.1	565±57	536±2	17.30	-12.91	
J0928+2845	SDSS	dI	09 28 59.06	+28 45 28.5	1229±41	1224±7	16.76	-14.82	
J0929+1155	SDSS	dI	09 29 51.83	+11 55 35.7	1349±51	1614±8	17.20	-14.84	
J0931+2717	SDSS	Sm:	09 31 36.15	+27 17 46.6	1505±2	1504±3	18.00	-13.94	
J0934+0625*	CGCG035-007	Sc	09 34 44.72	+06 25 31.2	574±38	548±4	15.42	-14.50	PC 0956+4751
J0937+2733	SDSS	Im	09 37 47.65	+27 33 57.7	1595±16	1588±1	16.50	-15.58	
J0940+4459	SDSS	dI	09 40 03.27	+44 59 31.7	1358±4	1350±10	18.01	-13.79	
J0942+09375*	SDSS	dI	09 42 51.25	+09 37 57.6	1461±17	1456±6	18.15	-13.67	
J0943+4134	SDSS	dI	09 43 42.97	+41 34 08.9	1403±40	1436±4	17.64	-14.25	
J0944+1000	SDSS	dI	09 44 37.10	+10 00 46.3	1477±66	1476±3	16.96	-14.89	PC 0956+4751
J0947+4138	SDSS	BCG	09 47 18.35	+41 38 16.4	1389±2	1400±2	17.92	-13.93	
J0947+3905a*	MRK407	BCG	09 47 47.60	+39 05 03.0	1589±10	1582±4	15.28	-16.79	
J0947+3908*	UZC	Sd	09 47 50.25	+39 08 31.7	1553±25	1565±4	16.85	-15.20	
J0947+3905b	SDSS	LSB	09 47 58.45	+39 05 10.1	1501±60	1567±4	18.03	-14.02	
J0951+3842	SDSS	dI	09 51 41.67	+38 42 07.3	1435±4	1433±7	17.46	-14.43	PC 0956+4751
J0954+3620	SDSS	dI	09 54 50.60	+36 20 01.9	503±55	550±5	18.05	-12.17	
J0956+2716*	SDSS	dI	09 56 33.65	+27 16 59.3	1074±25	1059±2	18.13	-13.17	
J0957+2745*	SDSS	dI	09 57 29.40	+27 45 24.3	1184±16	1184±4	18.16	-13.33	
J0959+4736	SDSS	dI	09 59 18.60	+47 36 58.4	1093±4	1110±12	17.05	-14.37	
J1000+3032	SDSS	dI	10 00 36.54	+30 32 09.8	501±37	484±13	18.14	-11.87	PC 0956+4751
J1010+4617	SDSS	dI	10 10 14.96	+46 17 44.1	1092±3	1092±3	18.23	-13.15	
J1019+2923	SDSS	dI	10 19 28.52	+29 23 02.3	874±43	885±4	17.48	-13.60	

⁽¹⁾ – probable artifact. See text in Sect. 4.

Table 2. H I parameters of the observed Lynx-Cancer void sample galaxies

Short IAU style name (1)	$V(\text{HI}) \pm \sigma$ km s^{-1} (2)	Dist adopt (3)	$W_{50} \pm \sigma$ km s^{-1} (4)	$W_{20} \pm \sigma$ km s^{-1} (5)	$F(\text{HI}) \pm \sigma$ Jy km s^{-1} (6)	$\log \pm \sigma$ $M(\text{HI})$ (7)	$M(\text{HI}) \pm \sigma$ L_B (8)	Time min (9)	RMS mJy (10)	S/N (11)
J0626+2439	1485±2	23.21	138±3	156±5	7.04±0.22	8.95±0.013	3.20±0.100	42	3.5	16.2
J0629+2324	1445±2	22.92	129±3	150±4	10.40±0.25	9.11±0.010	3.69±0.090	22	4.1	22.2
J0713+2926	938±2	16.10	40±3	61±4	1.57±0.06	7.98±0.016	0.93±0.035	80	1.6	24.0
J0723+3621*	917±1	16.00	100±4	122±6	3.74±0.18	8.35±0.021	2.93±0.143	64	3.4	17.2
J0723+3622*	970±1	16.00	45±10	69±16	1.59±0.16	7.98±0.041	11.89±1.189	49	3.8	7.0
J0730+4109	878±5	15.75	51±10	72±16	0.74±0.10	7.64±0.056	0.41±0.056	84	2.4	6.0
J0737+4724	474±5	10.40	40±4	53±6	0.99±0.09	7.40±0.037	1.58±0.140	117	2.4	10.8
J0744+2508	760±3	13.10	28±6	43±9	0.39±0.05	7.20±0.052	0.88±0.113	128	1.7	7.5
J0744+2506	752±6	13.10	22±12	34±19	0.032±0.016	6.11±0.176	0.64±0.320	140	1.6	2.9
J0747+5111	433±3	9.92	75±5	105±9	5.96±0.27	8.14±0.019	0.77±0.035	26	5.2	15.4
J0802+0527	830±6	13.25	0.10±0.10	<6.62±0.301	<1.14±1.140	69	2.8	2.0
J0809+4135	712±5	13.48	95±10	137±16	5.13±0.30	8.34±0.025	0.97±0.057	19	5.1	12.0
J0810+1837	1481±8	23.03	42±15	64±24	0.46±0.09	7.76±0.079	1.37±0.274	25	2.3	4.4
J0812+4836	522±4	11.04	47±8	64±12	1.27±0.18	7.56±0.057	1.38±0.192	166	4.4	6.5
J0825+3201	647±6	12.23	62±12	84±18	1.11±0.17	7.59±0.062	0.82±0.126	37	3.7	5.6
J0831+4104	640±3	12.44	25±6	32±9	0.17±0.06	6.79±0.135	0.27±0.098	92	2.2	3.5
J0843+4025	627±10	12.23	24±21	46±33	0.19±0.09	6.83±0.168	0.37±0.175	63	2.8	3.2
J0845+1519	1584±12	24.19	6±24	39±38	0.10±0.05	7.14±0.176	0.39±0.195	175	1.6	4.1
J0852+1350	1502±8	22.96	77±15	118±24	2.30±0.22	8.46±0.039	2.75±0.261	20	4.0	8.0
J0859+3923	568±3	11.36	31±7	46±11	0.60±0.09	7.26±0.064	0.65±0.103	54	2.8	6.5
J0900+3222	740±30	13.18	0.14±0.10	<6.76±0.231	<0.72±0.520	35	3.4	1.4
J0911+3135	753±6	13.56	27±12	52±18	0.48±0.07	7.32±0.061	1.14±0.171	85	2.0	6.5
J0917+2525	1643±12	25.45	98±24	131±38	0.81±0.16	8.09±0.079	0.05±0.010	23	2.8	4.1
J0926+3343	536±2	10.63	43±4	79±7	2.71±0.10	7.86±0.015	3.23±0.117	72	2.2	24.4
J0928+2845	1224±7	19.84	94±14	123±22	1.99±0.26	8.27±0.053	1.41±0.182	17	4.6	6.3
J0929+1155	1614±8	24.29	119±15	138±24	3.14±0.17	8.64±0.023	3.27±0.178	37	2.9	3.7
J0931+2717	1504±3	23.59	48±6	71±10	0.54±0.13	7.85±0.092	1.21±0.285	47	3.0	11.0
J0934+0625	548±4	8.88	86±8	116±12	4.07±0.22	7.88±0.023	0.77±0.042	34	4.1	11.4
J0937+2733	1588±1	25.08	33±2	52±3	3.04±0.12	8.66±0.016	1.71±0.065	38	3.2	27.1
J0940+4459	1350±10	22.25	30±16	50±25	0.11±0.05	7.11±0.163	0.25±0.114	77	2.8	1.3
J0942+0937	1456±6	21.93	43±13	63±20	0.55±0.05	7.80±0.041	1.37±0.137	26	2.4	5.0
J0943+4134	1436±4	23.33	46±9	64±13	0.43±0.06	7.74±0.060	0.70±0.104	71	1.6	6.3
J0944+1000	1476±3	22.21	64±6	87±9	2.23±0.14	8.41±0.027	1.84±0.116	21	3.0	12.1
J0947+4138	1400±2	22.71	61±3	90±5	0.20±0.07	7.39±0.132	0.42±0.149	132	1.5	27.9
J0947+3905a	1582±4	25.11	157±7	193±12	7.00±0.50	9.02±0.030	1.29±0.092	22	3.3	27.0
J0947+3908	1565±4	25.11	5.00±0.40	8.87±0.033	3.92±0.314	20	3.0	22.0
J0947+3905b	1567±4	25.11	1.50±0.20	8.35±0.054	3.48±0.464	20	3.0	21.0
J0951+3842	1433±7	23.04	29±14	56±22	0.48±0.11	7.78±0.089	0.65±0.148	48	2.9	5.7
J0954+3620	550±5	10.86	44±10	63±15	0.28±0.05	6.89±0.074	0.68±0.126	86	1.3	6.0
J0956+2716**	1059±2	19.94	56±5	68±8	1.46±0.12	8.14±0.035	1.90±0.161	44	3.0	10.9
J0957+2745	1184±4	19.14	40±9	52±13	0.33±0.07	7.46±0.086	0.86±0.188	45	2.1	4.2
J0959+4736	1110±12	18.89	80±24	134±37	1.91±0.16	8.21±0.036	1.80±0.154	47	3.6	6.8
J1000+3032	484±13	9.68	34±25	55±39	0.15±0.07	6.52±0.166	0.38±0.177	29	2.5	3.0
J1010+4617	1092±3	18.57	0.06±0.06	<6.69±0.301	<0.34±0.340	37	2.4	2.0
J1019+2923	885±4	15.40	71±8	86±12	1.04±0.13	7.77±0.051	1.36±0.170	23	2.8	5.8

(*) – H I parameters are adopted based on GMRT data from Chengalur, Pustilnik (2013);

(**) – distance as for IC2520=J0956+2713, a massive component of pair with $V_{\text{hel}}=1243 \text{ km s}^{-1}$.

